JJEE
Volume 7, Number 2, June 2021
Pages 96-107
Jordan Journal of Electrical Engineering
ISSN (Print): 2409-9600, ISSN (Online): 2409-9619

OFDM System with Half-Symbol-Spaced Receiver and Channel Acquisition Error over Multipath Fading Channels

Ali Alqatawneh[1*], Luae Al-Tarawneh[2]

[1] Communications and Computer Engineering Department, Tafila Technical University, Tafila, Jordan
E-mail: ali.katawneh74@gmail.com
[2] Communications Engineering Department, Princess Sumaya University for Technology, Amman, Jordan.

Received: February 15, 2021 *Revised: March 03, 2021* *Accepted: March 07, 2021*

***Abstract*—** In this paper, we study the orthogonal frequency division multiplexing (OFDM) system under imperfect channel-acquisition. We consider an OFDM system with a half-symbol-spaced receiver, where we employ a pilot symbol padding scheme for channel acquisition. Also, we use the Kronecker tensor product either at the transmitter to insert pilot symbols among data symbols or at the receiver to extract signals associated with pilots or data symbols. Also, we obtain the symbol detection with the minimal probability of error under imperfect channel acquisition. Results, both simulation and analytical, reveal that channel acquisition error degrades the system performance. However, the OFDM system with a half-symbol-spaced receiver shows better error probability and less acquisition error compared to the OFDM system with a symbol-spaced receiver.

***Keywords*—** Orthogonal frequency division multiplexing system; Half-symbol-spaced receiver; Pilot percentage; Channel acquisition; Pilot padding; Mean-squared error.

Nomenclature

$\mathbf{I}_a$	Identity matrix of size a
$\mathbf{u}_{2N}$	All-ones column vector of length $2N$
$\boldsymbol{\beta}_{1xb}$	Row vector of length b and zero elements except the last element which equals one
$\boldsymbol{\varphi}_{1\times N}^{k}$	Row vector of length N with zero elements except for the k-th element which equals one
$\mathcal{C}^{a\times b}$	Complex matrix with a rows and b columns
$\mathbf{0}_{axb}$	Null matrix with a rows and b columns
$\otimes$	The Kronecker tensor product
$\mathbf{E}[X]$	Expectation of the random variable X
$()^T$	The matrix transpose
$()^*$	The Hermitian transpose

1. INTRODUCTION

Orthogonal frequency division multiplexing (OFDM) has been widely applied in wireless communication systems because of its robustness against frequency selective multipath fading and its high efficiency bandwidth. Furthermore, the OFDM can be easily realized using an Inverse Fast Fourier Transform (IFFT) at the transmitter and a Fast Fourier Transform (FFT) at the receiver [1, 2].

* Corresponding author
Article's DOI: 10.5455/jjee.204-1613432117

In wireless communication over multipath fading channels, a powerful channel acquisition technique is essential for correct OFDM signal detection at the receiver. Thus, a precise channel acquisition is crucial to maintain reliable and high-quality wireless communication services over multipath fading channels. However, due to fast fading fluctuations in frequency of selective fading channels, channel acquisition with high accuracy is a difficult task. In the OFDM system, channel acquisition can be implemented by adding extra pilot tones. In this scheme, channel coefficients are initially estimated at pilot tones, the estimated channel coefficients are then utilized to acquire channel coefficients at subcarriers associated with data symbols [3]. To address different types of fading channels, pilot tones can be either inserted into all of the OFDM subcarriers to address slow fading fluctuations or inserted into every OFDM symbol to address fast fading channel variations [3]. Inserting equal-spaced pilot tones into every OFDM symbol improves the tracking of channel variations leading to channel acquisition accuracy enhancement [4]. In [5], a pilot-assisted channel estimation analysis is performed for the OFDM system in multipath Rayleigh-fading channels; however, the analysis is performed under noise-free conditions. In the OFDM system with a noise-restricted channel, the pilot-assisted channel acquisition scheme will enhance the error performance as shown in [6]. For the OFDM system with known channel statistics, the channel acquisition errors can be significantly reduced by incorporating a linear minimum mean-squared error (LMMSE) estimator [7]. Besides, the computational complexity of the LMMSE estimator can be reduced using the singular value decomposition (SVD) at the expense of increasing the performance attenuation [8]. In the OFDM system with time-varying fading channels, the frequency domain channel matrix has a non-diagonal structure; therefore, the accuracy of channel acquisition will be adversely affected by the interference [9]. Increasing the number of inserted pilot symbols among data symbols rises the accuracy of channel acquisition. However, this improvement occurs at the expense of increasing the overhead which decreases the spectral efficiency of the OFDM system [10-13].

According to [14], the symbol error probability of the OFDM system can achieve considerable improvement by upsampling the OFDM received signal, in time domain, at a rate of twice the transmitter rate. The upsampling in time-domain originates diversity enhancement at the receiver. Besides, wireless communication systems with upsampling are robust against the adverse impacts of the sampler's timing mismatching between the transmitter and the receiver [14, 15]. The authors in [14] assume that the channel information is perfectly known at the receiver side. However, this assumption is difficult to satisfy in practical wireless communication systems. Thus, in this paper, we examine an upsampled OFDM system under channel acquisition errors and noise. We use an upsampling with factor of two where the system can be considered as an OFDM system with a half-symbol-spaced receiver. Also, we study the impact of having a half-symbol-spaced receiver on the channel acquisition errors. We employ a pilot-padding channel acquisition technique where we use the received pilot signals to acquire channel coefficients associated with data symbols [13]. We use the Kronecker tensor product either at the transmitter to insert pilot symbols among data symbols or at the receiver to extract signals associated with pilots or data symbols. Finally, we derive the optimum detection for the OFDM system with a half-symbol-spaced receiver under channel acquisition errors.

The remainder of this paper is structured as follows: section 2 formulates the problem. In section 3, receiver analysis is presented. Results and discussions are shown in section 4. Finally, this paper is concluded in section 5.

2. POBLEM FORMULATION AND CHANNEL ACQUISITION

2.1. Problem Formulation

Consider an OFDM system with a half-symbol-spaced receiver, where an equally-spaced pilot-padding channel acquisition technique with N_p pilot symbols is used. At the transmitter, for every information slot, with K symbols, a pilot symbol is added to formulate symbols segment with length N, where $N = K(N_p+1)$. The pilot padding process can be represented in matrix format as:

$$\mathbf{s} = (\mathbf{s}_d\mathbf{C}_d + \mathbf{s}_p\mathbf{C}_p)^T \quad (1)$$

where $\mathbf{s}_d$ =[$s(1)$, $s(2)$,…, $s(KN_p)$] is the data symbols sequence row vector before pilots insertion, $\mathbf{s}_p$ =[$p(1)$, $p(2)$,…, $p(N_p)$] is the pilot symbols sequence row vector, the vector $\mathbf{s}$ represents the data symbols after pilots insertion and serial to parallel conversion, $\mathbf{C}_d = \mathbf{I}_{N_p} \otimes [\mathbf{I}_K | \mathbf{0}_{K\times 1}]$, and $\mathbf{C}_p = \mathbf{I}_{N_p} \otimes \boldsymbol{\beta}_{1\times(K+1)}$ are the pilot symbols padding matrices with sizes of $2N_p\times N$ and $2N_pK\times N$, respectively. All symbols in the vector $\mathbf{s}$ are drawn from an M-array phase shift modulation (MPSK) constellation. For illustration purpose, let us assume that K= 3, and N_p= 4, then the pilot padding can be graphically represented as in Fig. 1.

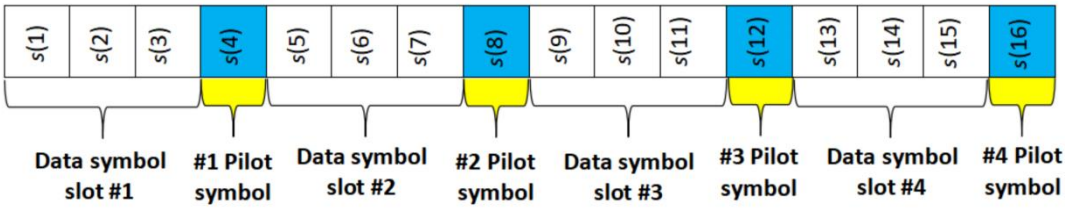

Fig. 1. Pilot padding illustration example.

The vector $\mathbf{s}$ is then used to modulate an N-orthogonal subcarriers using N-point inverse Fast Fourier Transform ($IFFT_N$) resulting time domain OFDM samples vectors $\mathbf{x}$=[$x(1)$, $x(2)$, . . ., $x(N)$]^T as shown in Fig. 2.

A cyclic prefix sequence was incorporated to the OFDM samples in order to avoid block interference. The samples are then moved through a square-root raised-cosine pulse shaping filter. After filtering, the signal is transmitted to the destination over multipath fading channel and corrupted by an additive white Gaussian noise (AWGN) with variance N_0. After filtering, the signal is sampled at a rate that is half the rate of the transmitter. In a matrix representation and after the cyclic prefix removal, the sampled signal can be expressed as [14]:

$$\mathbf{r} = \mathbf{G} \,.\, \mathbf{IFFT_N}\,(\mathbf{s}) + \mathbf{n} \quad (2)$$

where $\mathbf{r} = [r(1),\cdots,r(2N)]^T$, $\mathbf{x} = \mathrm{FFT}_N\{\mathbf{s}\}$, $\mathbf{n} = [n(1),\cdots,n(2N)]^T$ is the time-domain noise vector, and $\mathbf{G} \in \mathcal{C}^{2N\times N}$ denotes the time-domain channel matrix [14]. After 2N-point FFT (FFT_{2N}) processing, the signal $\mathbf{r}$ can be described in frequency domain by:

$$\begin{aligned}\mathbf{y} &= \mathrm{FFT}_{2N}(\mathbf{r}) \\ &= \mathrm{FFT}_{2N}(\mathbf{G}\cdot\mathrm{IFFT}_{N}(\mathbf{I}_{N}))\mathbf{s} + \mathrm{FFT}_{2N}(\mathbf{n}) = \mathbf{H}\cdot\mathbf{s} + \mathbf{z},\end{aligned} \tag{3}$$

where $\mathbf{y} = \mathrm{IFFT}_{2N}\{\mathbf{r}\} \in \mathcal{C}^{2N\times 1}$, $\mathbf{z} = \mathrm{FFT}_{2N}\{\mathbf{n}\} \in \mathcal{C}^{2N\times 1}$, and $\mathbf{H} = \frac{1}{\sqrt{2}}\mathrm{FFT}_{2N}\{\mathbf{G}\cdot\mathrm{IFFT}_{N}(\mathbf{I}_{N})\} \in \mathcal{C}^{2N\times N}$ represents the channel matrix in the frequency domain. Eq. (3) can alternatively be expressed as $\mathbf{y} = (\mathbf{I}_2 \otimes \mathbf{S})\mathbf{h} + \mathbf{z}$, where $\mathbf{S}$ is a diagonal matrix with diagonal being the vector $\mathbf{s}$, and $\mathbf{h} = \mathbf{H}\cdot\mathbf{u}_{2N}$ is the channel coefficients vector. For convenience we assume that the average symbol energy is unity.

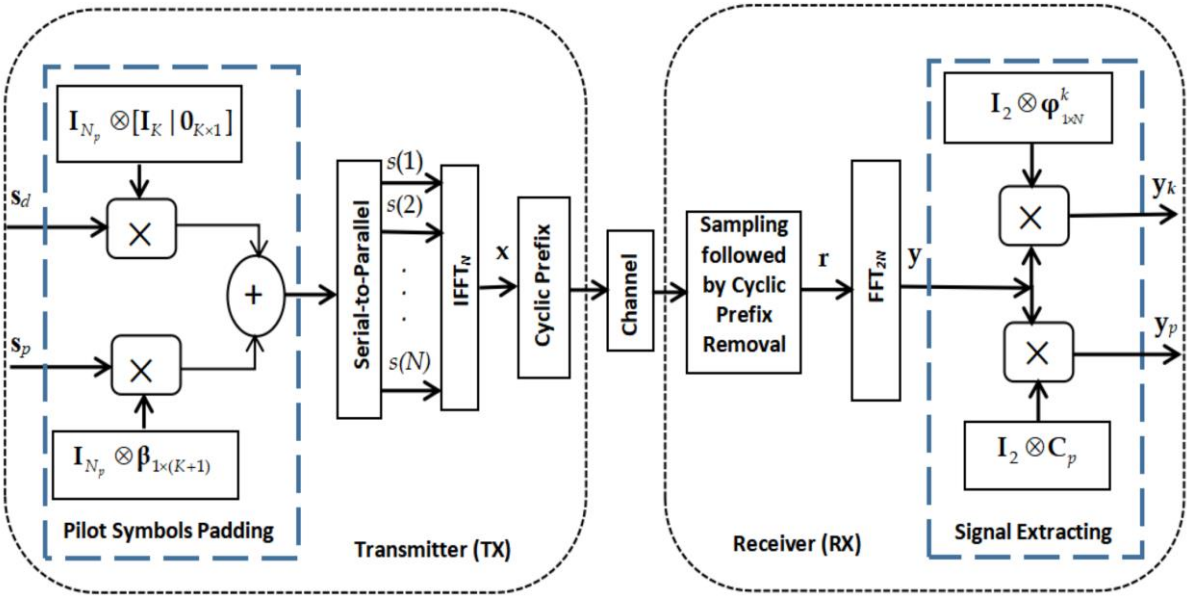

Fig. 2. Block diagram of the OFDM system with a half-symbol-spaced receiver and pilot-padding channel acquisition where the block "×" represents the matrix multiplication.

2.2. Channel Acquisition for the *k*-th Data Symbol

The received signal associated with pilot symbols is employed to acquire channel information associated with data symbols [11-13]. If we denote the signal related to pilot symbols as $\mathbf{y}_p \in \mathcal{C}^{2N\times 1}$, and the signal related to the *k*-th data symbol as $\mathbf{y}_k \in \mathcal{C}^{2N\times 1}$, then $\mathbf{y}_p$ and $\mathbf{y}_k$ can be respectively extracted from vector $\mathbf{y}$ as indicated below:

$$\mathbf{y}_p = \left(\mathbf{I}_2 \otimes \mathbf{C}_p\right)\mathbf{y}, \tag{4}$$

$$\mathbf{y}_k = \left(\mathbf{I}_2 \otimes \boldsymbol{\varphi}^k_{1\times N}\right)\mathbf{y}, \tag{5}$$

where $\mathbf{y}_p = \left[y(N_p), y(2N_p), \ldots, y(mN_p)\right]^T$, $m = 2N_p$ and $\mathbf{y}_k = \left[y(k), \cdots, y(k+N))\right]^T$ with $k \in \{0,2,\cdots,N-1\}$, and $k \notin \{1+K, 2+2K, \cdots, N_p + KN_p\}$. Alternatively, Eqs. (4) and (5) can be written as [12, 14]:

$$\mathbf{y}_p = \left[\mathbf{I}_2 \otimes \mathbf{S}_p\right]\cdot\mathbf{h}_p + \mathbf{z}_p, \tag{6}$$

$$\mathbf{y}_k = \mathbf{h}_k \cdot s(k) + \mathbf{z}_k, \tag{7}$$

where $\mathbf{h}_p = \left(\mathbf{I}_2 \otimes \mathbf{C}_p\right)\mathbf{h} \in \mathcal{C}^{2N_p\times 1}$, $\mathbf{h}_k = \left(\mathbf{I}_2 \otimes \boldsymbol{\varphi}^k_{1\times N}\right)\cdot\mathbf{h} \in C^{2\times 1}$ are channel vectors for the pilot and the *k*-th data symbols, respectively, $\mathbf{S}_p$ is a diagonal matrix with diagonal being $\mathbf{s}_p$,

and $s(k)$ denotes the k-th data symbol; $\mathbf{z}_p = \left(\mathbf{I}_2 \otimes \mathbf{C}_p\right)\mathbf{z} \in \mathcal{C}^{2N_P \times 1}$, $\mathbf{z}_k = \left[\mathbf{I}_2 \otimes \boldsymbol{\varphi}_{1\times N}^{k}\right]\mathbf{z} \in \mathcal{C}^{2\times 1}$ are the noise vectors related to the pilot and the k-th data symbols, respectively.

If we refer to the estimated channel coefficient at the k-th data symbol as $\hat{\mathbf{h}}_k$, the channel acquisition error is then $\mathbf{e}_k = \hat{\mathbf{h}}_k - \mathbf{h}_k$. The channel acquisition for the k-th data symbol can be achieved by using the orthogonality principle $\mathsf{E}[\mathbf{e}_k \mathbf{h}_k^*] = 0$ as [11-13]:

$$\hat{\mathbf{h}}_k = \mathbf{A}_{kp}\mathbf{S}_p^* \mathbf{A}_{y_p}^{-1}\mathbf{y}_p = \mathbf{A}_{kp}\mathbf{S}_p{}^* \left(\mathbf{S}_p \mathbf{A}_{pp}\mathbf{S}_p{}^* + \mathbf{R}_p\right)^{-1}\mathbf{y}_p \tag{8}$$

where $\mathbf{A}_{kp} = \mathsf{E}(\mathbf{h}_k \mathbf{h}_p^*) \in \mathcal{C}^{2\times 2N_P}$ is the cross-correlation matrix between $\mathbf{h}_k$ and $\mathbf{h}_p$ with the (m,n)-th element being $\mathbf{A}_{kp}(m,n) = \mathsf{E}(h_k(m)h_p^*(n))$, $\mathbf{A}_{pp} = \mathsf{E}(\mathbf{h}_p \mathbf{h}_p^*) \in \mathcal{C}^{2N_P \times 2N_P}$ is the auto-correlation matrix for channel coefficients associated with pilot symbols, and $\mathbf{R}_{y_p} = \mathsf{E}(\mathbf{y}_p \mathbf{y}_p^*) = \left(\mathbf{S}_p \mathbf{A}_{pp}\mathbf{S}_p^* + \mathbf{R}_p\right) \in \mathcal{C}^{2N_P \times 2N_P}$ with $\mathbf{R}_p = \mathsf{E}[\mathbf{z}_p \mathbf{z}_p^*] \in \mathcal{C}^{2N_p \times 2N_p}$ [11-13]. $\mathbf{A}_{pp}$ and $\mathbf{A}_{kp}$ are found using the Kronecker tensor product as follows:

$$\mathbf{A}_{pp} = \left(\mathbf{I}_2 \otimes \mathbf{C}_p\right)\mathbf{A}_{hh}\left(\mathbf{I}_2 \otimes \mathbf{C}_p\right)^T \tag{9}$$

$$\mathbf{A}_{kp} = \left(\mathbf{I}_2 \otimes \boldsymbol{\varphi}_{1\times N}^{k}\right)\mathbf{A}_{hh}\left(\mathbf{I}_2 \otimes \mathbf{C}_p\right)^T \tag{10}$$

where $\mathbf{A}_{hh} = \mathsf{E}(\mathbf{h}\mathbf{h}^*) \in \mathcal{C}^{2N\times 2N}$ is the auto-correlation matrix of the channel coefficient vector $\mathbf{h}$. Based on [13], the mean-squared error for the channel acquisition of the k-th data symbol is evaluated as $\Delta_k = \frac{1}{2}\sum_{m=1}^{2}\mathsf{E}(|e_k(m)|^2)$, which also can be written as:

$$\Delta_k = \tfrac{1}{2}\, trace(\mathbf{A}_e), \tag{11}$$

where $\mathbf{A}_e = \mathsf{E}\left[\mathbf{e}_k \mathbf{e}_k^*\right] = \mathsf{E}\left[\left(\hat{\mathbf{h}}_k - \mathbf{h}_k\right)\left(\hat{\mathbf{h}}_k - \mathbf{h}_k\right)^*\right] \in \mathcal{C}^{2\times 2}$ is the error auto-correlation matrix. We can use $\mathbf{A}_{pp}$ and $\mathbf{A}_{kp}$ to identify the $\mathbf{R}_e$ matrix as shown below:

$$\begin{aligned}\mathbf{A}_e &= \mathbf{A}_{kk} - \mathbf{A}_{kp}\mathbf{S}_p^*\mathbf{R}_{y_p}^{-1}\mathbf{S}_p\mathbf{A}_{kp}^* \\ &= \mathbf{A}_{kk} - \mathbf{A}_{kp}\mathbf{S}_p^*\left(E_p\mathbf{S}_p\mathbf{A}_{pp}\mathbf{S}_p^* + \mathbf{R}_p\right)^{-1}\mathbf{S}_p\mathbf{A}_{kp}^* \\ &= \mathbf{A}_{\hat{k}\hat{k}}\end{aligned} \tag{12}$$

where $\mathbf{A}_{kk} \in \mathcal{C}^{2\times 2}$ is the auto-correlation matrix for channel coefficients of the k-th data symbol. Using the Kronecker tensor product $\mathbf{A}_{kk}$ can be represented as:

$$\begin{aligned}\mathbf{A}_{kk} &= \mathsf{E}\left[\left(\left[\mathbf{I}_2 \otimes \boldsymbol{\varphi}_{1\times N}^{k}\right]\cdot \mathbf{h}\right)\left(\left[\mathbf{I}_2 \otimes \boldsymbol{\varphi}_{1\times N}^{k}\right]\cdot \mathbf{h}\right)^*\right] \\ &= \left(\mathbf{I}_2 \otimes \boldsymbol{\varphi}_{1\times N}^{k}\right)\mathsf{E}\left(\mathbf{h}\mathbf{h}^*\right)\left(\mathbf{I}_2 \otimes \boldsymbol{\varphi}_{1\times N}^{k}\right)^T \\ &= \left(\mathbf{I}_2 \otimes \boldsymbol{\varphi}_{1\times N}^{k}\right)\mathbf{A}_{hh}\left(\mathbf{I}_2 \otimes \boldsymbol{\varphi}_{1\times N}^{k}\right)^T\end{aligned} \tag{13}$$

3. SIGNAL DETECTION AND SYMBOL ERROR PROBABILITY ANALYSIS

3.1. Signal Detection in the Presence of Channel Acquisition Errors

The received signal associated with the k-th data symbol was obtained using the Kronecker tensor product as shown in Eq. (7). The noise samples at the sampler output for the

half-symbol-spaced receiver are correlated. This correlation between different noise samples should be removed before using the maximum ratio combining [14, 16]. Fortunately, the correlation can be eliminated by multiplying both sides of the Eq. (7) by $\sqrt{N_0}(\mathbf{R}_k)^{-\frac{1}{2}}$, where $\mathbf{R}_k = \mathrm{E}[\mathbf{z}_k \mathbf{z}_k^*] \in \mathcal{C}^{2\times 2}$. After correlation elimination, Eq. (7) becomes:

$$\tilde{\mathbf{y}}_k = \sqrt{N_0}\mathbf{R}_k^{-\frac{1}{2}}\mathbf{y}_k = \sqrt{N_0}\mathbf{R}_k^{-\frac{1}{2}}\mathbf{h}_k \cdot s(k) + \sqrt{N_0}(\mathbf{R}_k)^{-\frac{1}{2}}\mathbf{z}_k \tag{14}$$

For the sake of brevity, we do not mention the proof.

The detection of the *k*-th data symbol is performed after receiving $\tilde{\mathbf{y}}_k$ and obtaining $\hat{\mathbf{h}}_k$. If $\mathbf{h}_k$ in Eq. (14) is conditioned on $\hat{\mathbf{h}}_k$, then $\mathbf{h}_k$ is Gaussian distributed with mean vector and covariance matrix given respectively as [13]:

$$\mathbf{m}_{h_k/\hat{h}_k} = \mathrm{E}[\mathbf{h}_k / \hat{\mathbf{h}}_k] = \mathrm{E}[\mathbf{h}_k /(\mathbf{h}_k + \mathbf{e}_k)] = \hat{\mathbf{h}}_k \tag{15}$$

$$\begin{aligned}\mathbf{R}_{h_k/\hat{h}_k} &= \mathrm{E}\left[\left(\mathbf{h}_k - \mathrm{E}[\mathbf{h}_k / \hat{\mathbf{h}}_k]\right)\left(\mathbf{h}_k - \mathrm{E}[\mathbf{h}_k / \hat{\mathbf{h}}_k]\right)^*\right] \\ &= \mathrm{E}\left[\left(\mathbf{h}_k - \hat{\mathbf{h}}_k\right)\left(\mathbf{h}_k - \hat{\mathbf{h}}_k\right)^*\right] = \mathbf{R}_e.\end{aligned} \tag{16}$$

If the information bits are generated with the same probability, then the *k*-th data symbol can be detected with minimum probability of error by using the maximum likelihood estimation [13, 16] as:

$$\hat{s}(k) = (\tilde{\mathbf{y}}_k - \mathbf{m}_k)^* \mathbf{R}_{\tilde{y}_k}^{-1}(\tilde{\mathbf{y}}_k - \mathbf{m}_k) \tag{17}$$

where $\mathbf{m}_k$ refers to the mean of $\tilde{\mathbf{y}}_k$ conditioned on $\hat{\mathbf{h}}_k$, and $\mathbf{R}_{\tilde{y}_k} = \mathrm{E}[(\tilde{\mathbf{y}}_k \tilde{\mathbf{y}}_k^*)/\hat{\mathbf{h}}_k]$ indicates the covariance of $\tilde{\mathbf{y}}_k$ conditioned on $\hat{\mathbf{h}}_k$. Using Eqs. (14), (15), and (16), $\mathbf{m}_k$ and $\mathbf{R}_{\tilde{y}_k}$ can be derived as $\mathbf{m}_k = \sqrt{N_0}(\mathbf{R}_k)^{-\frac{1}{2}}\hat{\mathbf{h}}_k s(k)$ and $\mathbf{R}_{\tilde{y}_k} = \left(\left(\sqrt{N_0}(\mathbf{R}_k)^{-\frac{1}{2}}\right)\mathbf{R}_e\left(\sqrt{N_0}(\mathbf{R}_k)^{-\frac{1}{2}}\right)^* + N_o\mathbf{I}_2\right)$.

3.2. Symbol Error Probability Analysis

A mathematical expression of the symbol error probability (*PE*) of the system in Eq. (14) with MPSK and channel acquisition error is presented in this section. The *PE* is derived by finding the conditional error probability of the *k*-th symbol $PE_k / \hat{\mathbf{h}}_k$, then taking the expectation of $PE_k / \hat{\mathbf{h}}_k$. Based on [16], and Eq. (21) in [13], the conditional error probability of the symbol detection in Eq. (14) can be described by:

$$P_{k/\hat{\mathbf{h}}_k} = \frac{1}{\pi}\int_0^{\pi-\frac{\pi}{M}} exp\left[-E_s\hat{\mathbf{h}}_k^*(\sqrt{N_0}(\mathbf{R}_k)^{-\frac{1}{2}})^*\mathbf{R}_{\tilde{y}_k}^{-1}(\sqrt{N_0}(\mathbf{R}_k)^{-\frac{1}{2}})\hat{\mathbf{h}}_k \frac{sin^2(\frac{\pi}{M})}{sin^2(\theta)}\right]d\theta \tag{18}$$

Furthermore, by utilizing the eigenvalue decomposition mentioned in [13, 16] the unconditional probability of error for the *k*-th data symbol is given:

$$PE_k = \mathrm{E}[PE_k / \hat{\mathbf{h}}_k] = \frac{1}{\pi}\int_0^{\pi-\frac{\pi}{M}}\left\{\left[\frac{\sin^4(\theta)}{\left(\sin^2(\theta) + D_1\sin^2\left(\frac{\pi}{M}\right)\right)\left(\sin^2(\theta) + D_2\sin^2\left(\frac{\pi}{M}\right)\right)}\right]\right\}d\theta, \tag{19}$$

where D_1 and D_2 are the eigenvalues of the following matrix [13]:

$$\mathbf{A}_{\hat{k}\hat{k}}\left(\sqrt{N_0}(\mathbf{R}_k)^{-\frac{1}{2}}\right)^{*}\left(\left(\sqrt{N_0}(\mathbf{R}_k)^{-\frac{1}{2}}\right)\mathbf{R}_e\left(\sqrt{N_0}(\mathbf{R}_k)^{-\frac{1}{2}}\right)^{*}+\frac{\mathbf{I}_2}{\gamma}\right)^{-1}\left(\sqrt{N_0}(\mathbf{R}_k)^{-\frac{1}{2}}\right) \quad (20)$$

where $\gamma=\frac{1}{N_0}$ .Using PE_k given in Eq. (19), the resulting PE for the OFDM system with a half-symbol-spaced receiver and channel acquisition error is given below as [14]:

$$PE=\sum_{k=1,k\neq k_p}^{N}PE_k, k_p=m(K+1), m=1,2,\cdots,N_p \quad (21)$$

4. RESULTS AND DISCUSSION

In this section, we present MATLAB simulations to authenticate the aforementioned derived-theoretical results. We have performed simulations for OFDM systems with MPSK modulation under different signal-to-noise ratios (SNR) denoted by (γ) and channel acquisition errors. For comparison purposes, we denote the OFDM system with a half-symbol-spaced receiver as OFDM-2, while we refer to the OFDM system with the symbol-spaced receiver as OFDM. In all simulations, we have considered transmission over noise and a quasi-static multipath fading channel with typical urban area power delay profile [17].

In Fig. 3, the *PE*s for the OFDM-2 system under perfectly-known channel coefficients assumption are compared with *PE*s for an equivalent one with imperfect channel acquisition. In the same figure, we also plot the *PE*s for the OFDM system under identical conditions for comparison aims. As predicted, the error performance of the OFDM-2 system surpasses that of the OFDM system even under perfectly-known channel assumption as stated in [14] or under channel acquisition errors as shown in the figure. Due to the reduction of channel acquisition errors, the *PE*s show improvement as the pilot percentage increases.

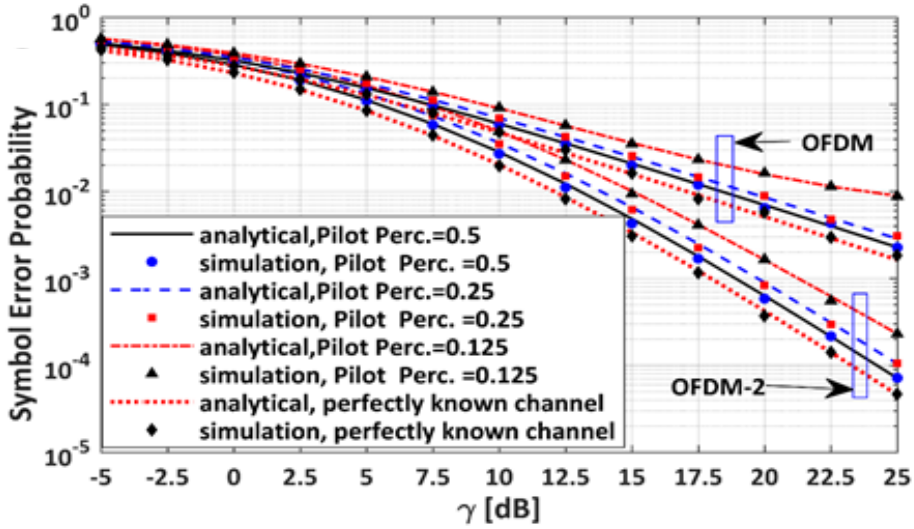

Fig. 3. The *PE*s for the OFDM-2 and OFDM systems as a function of γ (4PSK and *N=16* are considered for all systems).

For example and based on values withdrawn from Fig. 3, Table 1 compares the SNRs needed to reach *PE* of 10^{-2} at three pilot percentages; 0.5, 0.25, and 0.125 for OFDM and OFDM-2. As seen from the table, *PE*=10^{-2} can be reached at lower SNR for OFDM-2 compared to OFDM. The same thing is correct when the channel is perfectly known. The last

row in Table 1 shows the SNR difference between the two systems. At a pilot percentage of 0.125, where the channel acquisition error is at its highest level, the SNR difference is maximum and equals 8.5 dB. While the smallest SNR difference, which equals 5 dB, occurs when the channel is perfectly known, i.e., channel acquisition error is zero. Thus, using OFDM-2 can improve power efficiency, especially at low pilot percentage rates.

Table 1. The required SNR to reach *PE* of 10^{-2}.

	Perfectly known channel	Pilot percentage used for channel acquisition		
		0.5	0.25	0.125
SNR OFDM [dB]	17	18.5	19.5	23.5
SNR OFDM-2 [dB]	12	13	13.8	15
SNR OFDM -2- SNR OFDM [dB]	5	5.5	5.65	8.5

In Fig. 4, *PE*s are reported for OFDM-2 with 2PSK and 8PSK at different pilot symbol percentages. From the graph we can note that the symbol error probability of the OFDM-2 system with 2PSK is better than 8PSK. Increasing the pilot percentage improves performance for both 2PSK and 8PSK. For example, in OFDM-2 with 2PSK modulation, to reach a *PE* of (4.38×10^{-2}), the required SNR (γ) is 5 dB with perfectly-known channel coefficients, 5.85 dB with 0.5 pilot percentage, and 7.155 dB with 0.125 pilot percentage.

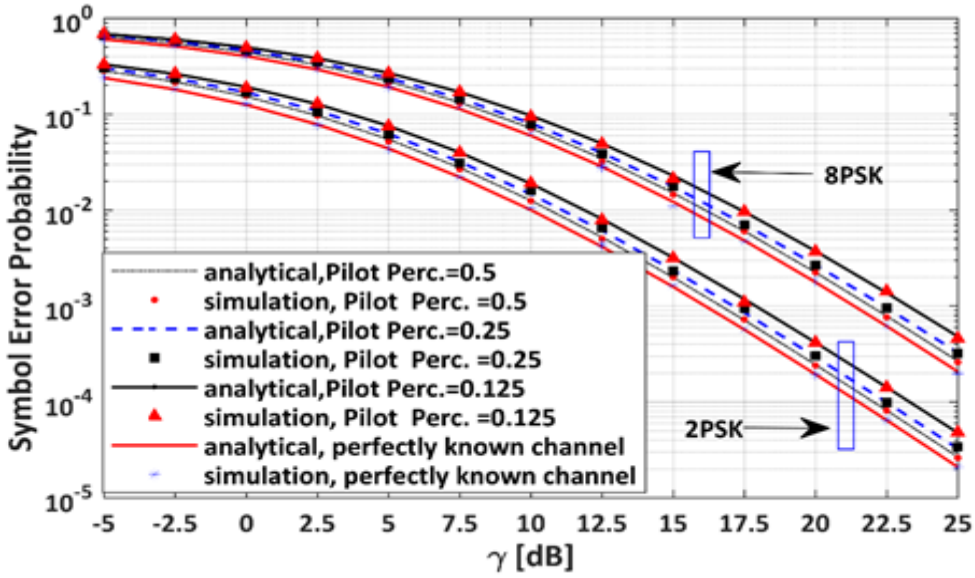

Fig. 4. *PE* of OFDM-2 with 2PSK and 8PSK as a function of γ (the number of orthogonal sub-carriers is 32 for all systems).

Likewise, in OFDM-2 with 8PSK, the *PE* at γ =5 dB is 1.1916×10^{-1} when the channel is perfectly-known; however, we can reach an identical symbol error probability at γ = 5.74 dB, and γ = 6.902 with pilot percentages equal to 0.5 and 0.125, respectively.

Fig. 5 provides the simulated mean-squared error (Δ_k) of the channel acquisition versus pilot symbol percentage (*Np/N*). In the figure, we also plot the Δ_k versus data symbol percentage (*KNp/N*).

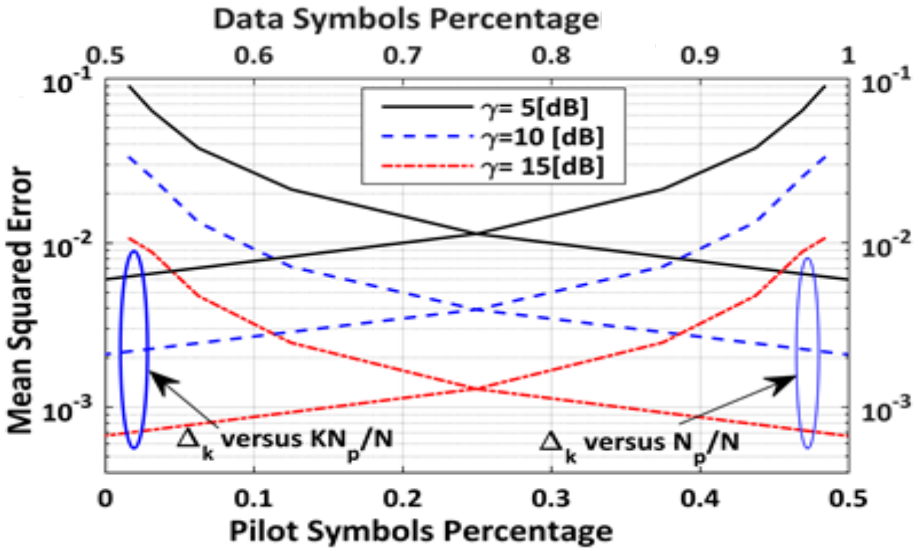

Fig. 5. The mean squared error (Δk) as a function of N_p/N, and as a function of KN_p/N.

It is apparent from this figure that increasing γ reduces channel estimation errors. Furthermore, as can be seen from the graph, channel acquisition error can be improved by increasing the pilot percentage and decreasing the data symbol percentage. Therefore, we need to make a trade-off between channel acquisition error and bandwidth utilization efficiency. The intersection between Δ_k versus the pilot percentage curve and Δ_k versus the data percentage curve defines a point where we have a small acquisition error at high data symbol percentage along with low pilot symbol percentage.

In Fig. 6, we plot the *PE* versus pilot symbol percentage (*Np/N*) for the OFDM-2 and the OFDM systems at various γ values. As Fig. 6 shows, there is a significant performance difference (at γ =10 dB) between the two systems. This significant difference is related to diversity enhancement in the OFDM-2 system due to half-symbol-spaced sampling [14].

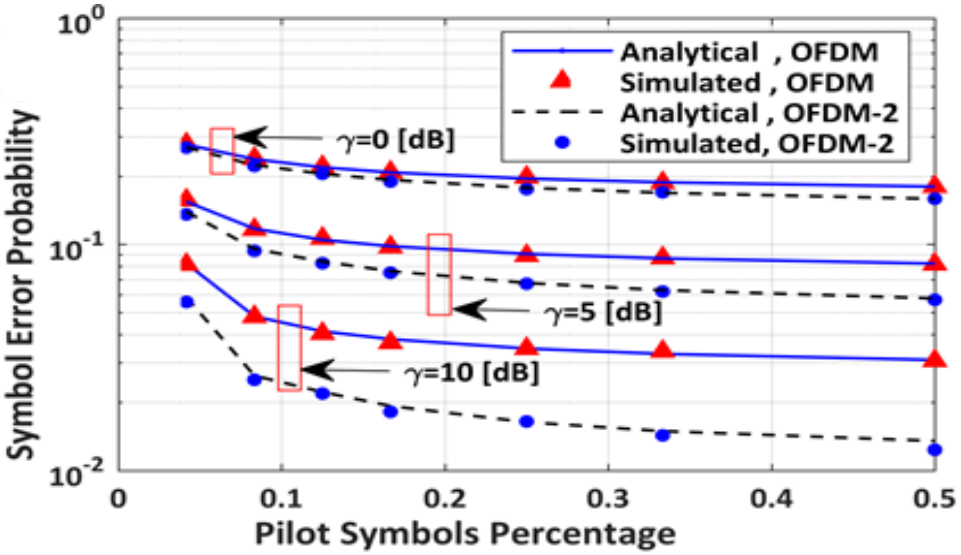

Fig. 6. The *PE*s for OFDM-2 and OFDM systems versus N_p/N (2PSK and N=24 are considered in each system).

In Fig. 7, the simulated mean-squared error for channel acquisition associated with the pilot symbols (Δ_p) and the k-th data symbols (Δ_k) are plotted for the OFDM-2 system as a function of γ under different numbers of subcarriers.

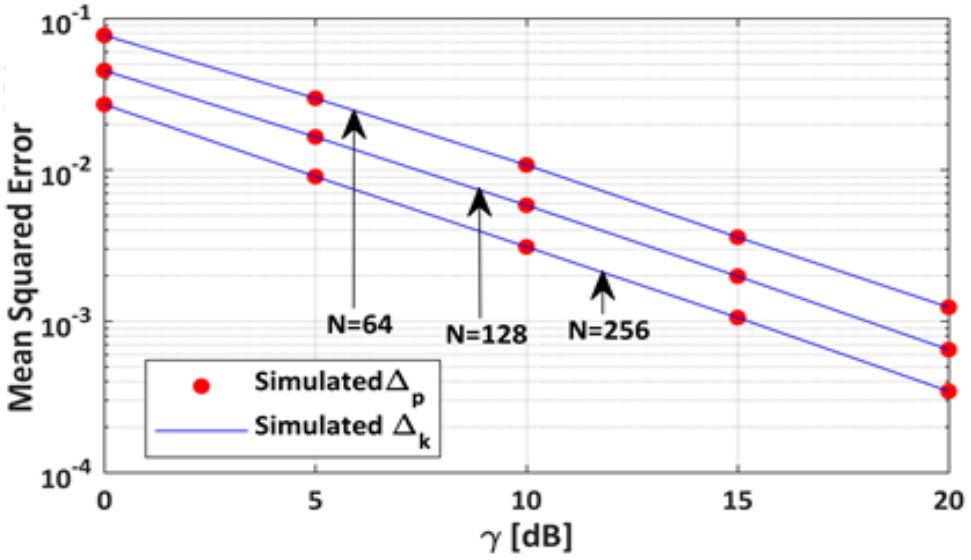

Fig. 7. The simulated Δ_k and Δ_p as a function of γ under various values of N (2PSK, K=3, and N_p/N=0.25 are used in all plots).

From the data in Fig. 7, it is apparent that the channel acquisition error can be reduced by increasing the length of the transmitted sequence (N). Increasing N means more transmitted pilot symbols, which leads to a reduction in Δ_k and Δ_p. Besides, increasing N decreases the needed SNR to reach certain Δ_k and Δ_p. For example, a mean-squared error of (3.1×10^{-3}) can be reached at 10 dB, 12.8 dB, 15.9 dB for N=256, N=128, and N=64, respectively.

Finally, Fig. 8 illustrates the impact of time-synchronization mismatching between the source and the destination on the mean-squared error of the channel acquisition for both OFDM-2 and OFDM systems. Binary phase shift keying (BPSK) , N=64, and N_p/N=0.25 are used to obtain the figure.

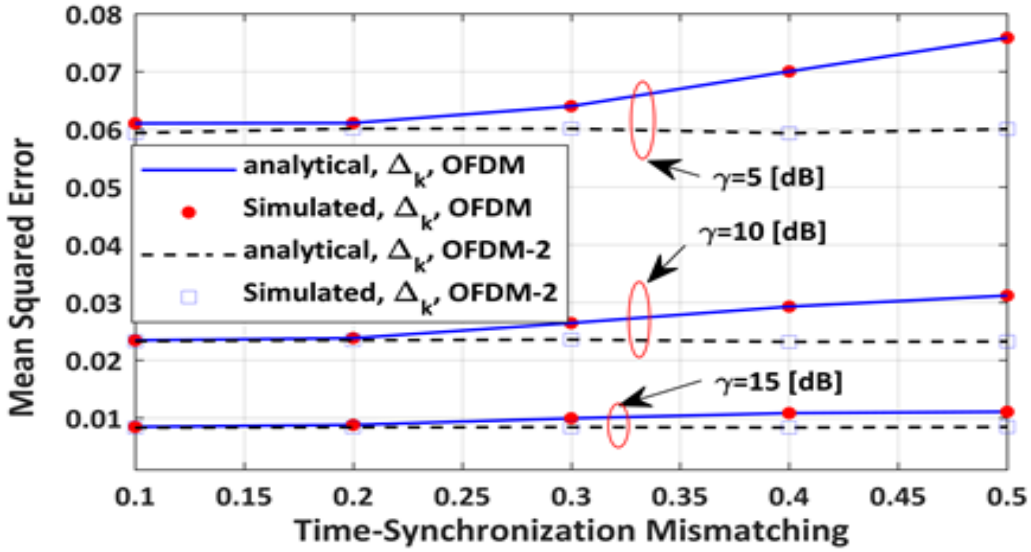

Fig. 8. The mean-squared error as a function of time-synchronization mismatching.

The analytical curves are plotted according to Eq. (11). As depicted in the figure, time-synchronization mismatching has no impact on the channel acquisition error in the OFDM-2 system, while time-synchronization mismatching increases the mean-squared error of channel acquisition in the OFDM system.

5. CONCLUSIONS

In this paper, we study the OFDM system with a half-symbol-spaced receiver under channel acquisition errors. The considered system employs a pilot-padding channel acquisition scheme in which the received signals associated with pilot symbols are employed to acquire channel information for the data symbols. We use the Kronecker tensor product to insert pilot symbols at the transmitter and to separate pilot symbols at the receiver. The impact of SNR, pilot percentage, and the number of used subcarriers on both the *PE* and the mean-squared error of channel acquisition are investigated. The outcomes demonstrate that using half-symbol-spaced sampling at the OFDM receiver has successfully enhanced both the *PE* and the channel acquisition. We also examined the impact of the SNR (γ), the pilot percentage, and the number of subcarriers on the system performance. The findings reveal that the acquisition mean-squared error and the *PE* improved by increasing one of the above parameters. Furthermore, the obtained results show that the OFDM with the half-symbol-spaced receiver can tackle any deviation caused by time synchronization-mismatching between the source and the destination.

REFERENCES

[1] A. Bingham, "Multicarrier modulation for data transmission: An idea whose time has come," *IEEE Communications Magazine*, vol. 28, no. 5, pp. 5-14, 1990.

[2] L. Cimini, "Analysis and simulation of a digital mobile channel using orthogonal frequency division multiplexing," *IEEE Transactions on Communications*, vol. 33, no. 7, pp. 665-675, 1985

[3] S. Colieri, M. Ergen, A. Puri, A. Bahai, "A study of channel estimation in OFDM systems," *Proceedings IEEE 56th Vehicular Technology Conference*, vol. 2, pp. 894-898, 2002.

[4] R. Negi, J. Cioffi, "Pilot tone selection for channel estimation in a mobile OFDM system," *IEEE Transactions on Consumer Electronics*, vol. 44, no. 3, pp. 1122-1128, 1998.

[5] B. Jiao, J. Xiao, J. Wang, "Analysis of channel estimation error of OFDM systems in Rayleigh fading," *International Symposium on Signals, Circuits and Systems*, vol. 2, pp. 653-656, 2005.

[6] Y. Li, "Pilot-symbol-aided channel estimation for OFDM in wireless systems," *IEEE Transactions on Vehicular Technology*, vol. 49, no. 4, pp. 1207–1215, 2000.

[7] Y. Liu, Z. Tan, H. Hu, L. Cimini, Y. Li, "Channel estimation for OFDM," *IEEE Communications Surveys and Tutorials*, vol. 16, no. 4, pp. 1891– 1908, 2014.

[8] T. Ma, Y. Shi, Y. Wang, "A low complexity MMSE for OFDM systems over frequency-selective fading channels," *IEEE Communications Letters*, vol. 16, no. 3, pp. 304–306, 2012.

[9] Z. Tang, R. Cannizzaro, G. Leus, P. Banelli, "Pilot-assisted time-varying channel estimation for OFDM systems," *IEEE Transactions on Signal Processing*, vol. 55, no. 5, pp. 2226–2238, 2007.

[10] M. Ozdemir, H. Arslan, "Channel estimation for wireless OFDM systems," *IEEE Communications Surveys and Tutorials,* vol. 9, no. 2, pp. 18–48, 2007.

[11] N. Sun, J. Wu, "On the performance of doubly-selective fading estimations in high mobility systems," *2014 IEEE 79th Vehicular Technology Conference*, pp. 1-5, 2014.

[12] N. Sun, J. Wu, "Maximizing spectral efficiency for high mobility systems with imperfect channel state information," *IEEE Transactions on Wireless Communications*, vol. 13, no. 3, pp. 1462–1470, 2014.

[13] W. Zhou, J. Wu, P. Fan, "Energy and spectral efficient Doppler diversity transmissions in high-mobility systems with imperfect channel estimation," *EURASIP Journal on Wireless Communications and Networking*, vol. 2015, no. 1, pp. 1-12, 2015.

[14] J. Wu, "Oversampled orthogonal frequency division multiplexing in doubly selective fading," *2008 IEEE Wireless Communications and Networking Conference*, pp. 177-181, 2008.

[15] J. Wu, Y. Zheng, K. Letaief, C. Xiao, "On the error performance of wireless systems with frequency selective fading and receiver timing phase offset," *IEEE Transactions on Wireless Communications,* vol. 6, no. 2, pp. 720–729, 2007.

[16] J. Wu, C. Xiao, "Performance analysis of wireless systems with doubly selective Rayleigh fading," *IEEE Transactions on Vehicular Technology*, vol. 56, no. 2, pp. 721–730, Mar. 2007.

[17] ETSI GSM 05.05, *Radio Transmission and Reception*, ETSI EN 300 910 V8.5.1, 2000.